International Journal of Pharmaceutics 703 (2026) 127299

Contents lists available at ScienceDirect

International Journal of Pharmaceutics

journal homepage: www.elsevier.com/locate/ijpharm

Photodynamic treatment of onychomycosis using bacterial nanocellulose patches for photosensitizer delivery

Francesca Mancusi [a], Mara Wesinger [b], Nidia Maldonado-Carmona [c], Elisa Bianchi [a], Giacomo Insero [c], Giovanni Romano [c], Barbara Richichi [a], Stefano Cicchi [a,*], Dagmar Fischer [b,d,**]

[a] Chemistry Department "Ugo Schiff", University of Florence, Italy
[b] Division of Pharmaceutical Technology and Biopharmacy, Friedrich-Alexander-Universität Erlangen-Nürnberg, Germany
[c] Biomedical Experimental and Clinical Sciences Department "Mario Serio", University of Florence, Italy
[d] FAU NeW - Research Center New Bioactive Compounds, Friedrich-Alexander-Universität Erlangen-Nürnberg, Germany

A B S T R A C T

The high prevalence of onychomycosis, a common pathology of nails due to fungal infections, has drawn attention to the development of new therapeutic approaches in which systemic secondary effects and the rise of drug resistance are avoided. Photodynamic therapy (PDT) is an approach that can be useful for treatment of onychomycosis, relying on the activation of a photosensitizer with light of a specific wavelength producing cytotoxic reactive oxygen species *in situ*. The present work describes the use of bacterial nanocellulose (**BNC**) patches delivering two different photosensitizers: Rose Bengal (**RB**) and a BODIPY derivative (**B-I$_2$**), whose differing hydrophilicity necessitated distinct formulation strategies. The experiments performed using vertical Franz cells allowed the optimization of the systems, finally tested in *in vitro* experiments with *Candida albicans* cultures. The results showed the efficacy of the BNC patches in the delivery of **RB**, showing that the presence of a keratolytic agent as urea is vital for the **RB** permeation through the nail models, with the permeation of **RB** being the first step for an efficient light-driven disinfection of *C. albicans* using green-laser light. Similar results were obtained with **B-I$_2$** although the high lipophilicity of the dye limited its cytotoxic evaluation *in vitro*.

1. Introduction

Onychomycosis is a fungal infection of the nails that leads to morphological changes such as discoloration, thickening, and onycholysis (Hoy et al., 2012). It is considered among the most common pathologies affecting the nail unit, caused by dermatophytes, non-dermatophyte moulds, and yeasts that produce keratolytic enzymes facilitating their entry and propagation (Gupta et al., 2023). All components of the nail unit can be involved, including the nail plate, nail matrix, and nail bed (Queller and Bhatia, 2015). The most common therapy involves the oral administration of antifungals such as terbinafine ("Terbinafine nail solutions for topical treatment of onychomycosis," 2013) or itraconazole (Zhang et al., 2018). However, these systemic drugs unfortunately have various side effects and are not indicated for all patient types. In some cases, topical therapy using medicated nail polishes or solutions based on, for example, efinaconazole, tavaborole, and ciclopirox, is preferred (Leung et al., 2020). These topical treatments are usually better tolerated by the patients, but the permeation of drug molecules through the nail plate, which is composed of a highly cross-linked keratin network, is often difficult. To overcome this problem, physical methods such as iontophoresis, ultrasound, and microperforation, often in combination with a partial removal of the nail plate, are employed to promote the entry of active molecules. Furthermore, formulation strategies, such as encapsulating active ingredients in nanoparticles and transferosomes, enhance their passage through the nail plate pores due to their small size. The incorporation of hydrating or keratolytic agents also represents a viable approach to increase nail plate penetration (Gupta et al., 2023). Unfortunately, the formation of fungal biofilms allows fungi to evade current antifungal therapies and contributes to antifungal resistance, highlighting the need for novel, more effective antifungal treatments (Gupta and Foley, 2019).

Photodynamic therapy (PDT) has been approved by the Food and Drug Administration (FDA) for the treatment of actinic keratoses and is used off-label for onychomycosis, being considered a simple, effective, and innovative method (Souza et al., 2014). Recent studies have shown that PDT is a valid alternative in the treatment of onychomycosis, either

* Corresponding author at: Chemistry Department "Ugo Schiff", University of Florence, Italy.
** Corresponding author at: Division of Pharmaceutical Technology and Biopharmacy, Friedrich-Alexander-Universität Erlangen-Nürnberg, Germany.
E-mail addresses: stefano.cicchi@unifi.it (S. Cicchi), dagmar.fischer@fau.de (D. Fischer).

https://doi.org/10.1016/j.ijpharm.2026.127299
Received 31 May 2026; Received in revised form 30 July 2026; Accepted 8 August 2026
Available online 10 August 2026

as monotherapy or in combination with systemic or topical antifungals, allowing the use of lower doses of the latter and thus reducing side effects (Navarro-Bielsa et al., 2022). PDT involves the use of photosensitizers (PSs) which, upon appropriate light irradiation, generate toxic reactive oxygen species (ROS), such as singlet oxygen ($^1O_2$) and hydroxyl radicals ($^{\cdot}OH$) (Shi et al., 2022). The photodynamic mechanism of fungal cell destruction occurs through oxidation of the cell wall and membrane, allowing the photosensitizer to further penetrate the cell. Subsequently, internal organelles such as lysosomes, mitochondria, and the nucleus are damaged, inducing cell death. The multiplicity of cellular targets reduces the risk of selecting resistant mutant strains (Calzavara-Pinton et al., 2012). **Rose Bengal** (**RB**, Fig. 1), a xanthene dye, activated with a 532 nm light, has shown to be an effective treatment for eradicating onychomycosis from toenails, *in vitro* and through a clinical approach (Houang et al., 2021). Characterized by an high singlet oxygen quantum yield, **RB** efficiency and safety are demonstrated by its current use in clinical practice and research. As an example, **RB** has been part of at least 9 clinical trials related to PDT since 2015, including several types of applications such as bacterial and fungal keratitis, metastatic tumours and different types of melanoma (National Library of Medicine, 2025). Recently, another class of compounds, known as BODIPYs (dyes with a 4,4-difluoro-4-bora-3a,4a-diaza-s-indacene core), have also been used following photoactivation to eradicate resistant pathogens and germs, demonstrating excellent results (Agazzi et al., 2019). Some derivatives have shown greater antifungal activity compared to traditional photosensitizers like 5-aminolevulinic acid (ALA), curcumin, and methylene blue (Wang et al., 2022). The versatility in BODIPY core functionalization, together with photostability make this class of compounds excellent candidates in PDT (Tricomi et al., 2025). Exploiting the potential of these photosensitizers in topical formulations that can improve their permeation through the nail plate would allow their possible use in PDT applied to onychomycosis (Shi et al., 2022).

Recently, bacterial nanocellulose (BNC) patches, supplemented with hydrating and keratolytic agents, have been used to improve the delivery of antifungal substances, significantly enhancing their permeation through the nail plate (Bellmann et al., 2022). BNC is produced through anaerobic fermentation of sugars by Gram-negative bacteria, for medical applications mainly of the genus *Komagataeibacter* (Klemm et al., 2006). It is an innovative biomaterial with a hydrophilic character, consisting of more than 90% water and characterized by a nanometric three-dimensional network that can host various active agents due to its high surface area (Jozala et al., 2016). Furthermore, its biocompatibility, high purity, exceptional mechanical stability and autoclavability make it ideal to produce medical devices (Liu et al., 2023; Pötzinger et al., 2019). Not surprisingly, BNC has recently been used to incorporate photosensitizers, enabling the development of antimicrobial wound dressings for light-driven disinfection (Sun et al., 2024; Zeng et al., 2024).

Our hypothesis was to verify if BNC patches can act as efficient systems for the transungual delivery of photosensitizers and if it is possible to optimize the process when using hydrophilic or hydrophobic photosensitizers.

In the present study, BNC patches containing **RB** and an azido-iodinated BODIPY derivative (Tricomi et al., 2025), **B-I$_2$** (Fig. 1) were formulated as delivery systems of photosensitizers for the local photodynamic treatment of onychomycosis. The introduction of heavy atoms, such as the two iodine atoms in the 2 and 6 positions, can also enhance the spin–orbit coupling within the photosensitizing molecules, significantly increasing the ability of organic PS to generate ROS (Li et al., 2026). The choice of the two different photosensitizers is related to their different physicochemical properties: **RB** is a highly water-soluble dye, well known in the literature and widely applied; on the contrary compound **B-I$_2$** is a new example of a rising class of more efficient photosensitizers, although with a marked lipophilic character and a reduced solubility in aqueous conditions. **B-I$_2$** and other BODIPY derivatives are the subject of another publication under process, but our unpublished results indicated that **B-I$_2$** is a more powerful and efficient photosensitizer than **RB**, although *in vitro* results against *C. albicans* rely on the use of an organic solvent, dimethyl sulfoxide, in the solution. These differences required the development of different loading strategies, offering the opportunity to widen the scope of the use of BNC patches. Two different agents, glycerol and propylene glycol (Carrer et al., 2020), acting as hydrating agents and penetration enhancer were added to the various formulations, while urea was included for its keratolytic properties with the aim to improve the permeation of the PSs through the nail plate (Björklund et al., 2013; Nguyen et al., 2021). The physicochemical characteristics of the BNC patches containing the

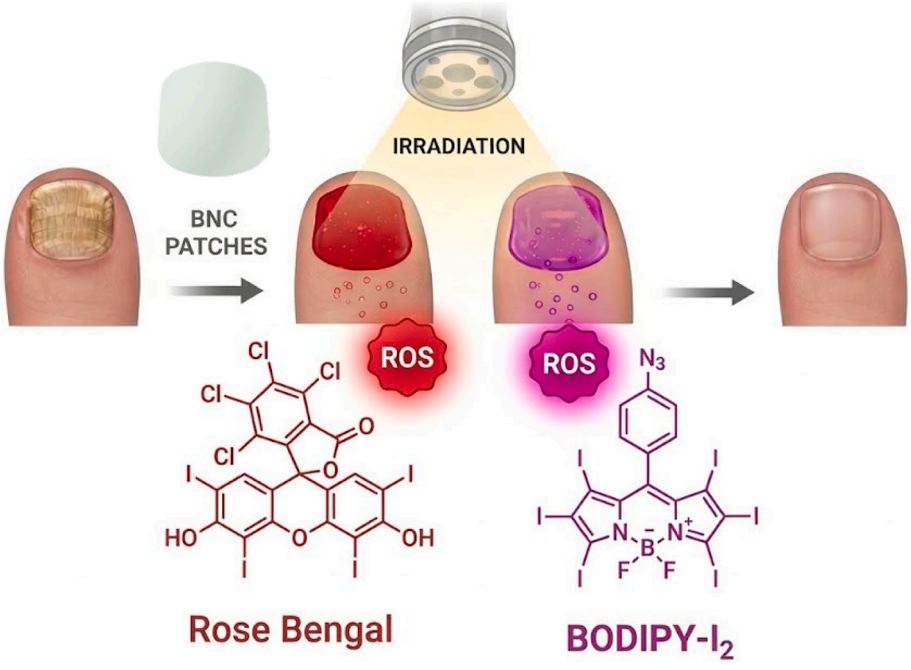

Fig. 1. PS molecules incorporated in BNC patches: **RB** and **B-I$_2$** (Image generated with Gemini 3 Flash).

photoactive molecules were studied, along with their release over time, their permeation through a nail model and their capacity to deliver the PS molecules for the photodynamic eradication of *Candida albicans*. *C. albicans* is an opportunistic yeast, which is a normal member of the skin microbiota but whom under the right circumstances can proliferate in healthy tissues (Sahoo et al., 2025), causing diverse pathologies such as candidiasis in the genitals and even onychomycosis, with the cases of yeast onychomycosis being less common than dermatophytes onychomycosis (Jaworek et al., 2025). Nevertheless, given our proof-of-concept approach, it was desirable to work with a well-established model before going for more exigent and challenging microorganisms, as dermatophytes are well known for a thicker cell wall and being able to produce pigments, which together make light delivery more difficult (Marques et al., 2025). The objective of this study is to exploit the capability of BNC patches as delivery system of **RB** and **B-I$_2$** photosensitizers via different formulation strategies and achieve effective treatment of yeast onychomycosis.

This manuscript introduces a photodynamic treatment for onychomycosis based on delivery with bacterial nanocellulose (BNC). The innovation lies in the application of a hydrophilic or a hydrophobic photosensitizer while preserving their photoactivity. The BNC matrix acts as a functional patch enhancing nail permeation and eradicating *Candida albicans*. These findings establish BNC for the first time as a biopolymer for the transungual delivery of photosensitizers with diverse structures.

2. Materials and methods

2.1. Reagents and materials

Rose Bengal (**RB**) was acquired from Thermo Fisher Scientific (Monza, Italy). Reagents involved in the synthesis of **B-I$_2$** were acquired from Sigma-Aldrich (Darmstadt, Germany). Phosphate-buffered saline pH 7.4, ethanol, sodium hydroxide, glycerol, urea, propylene glycol, tris, thiourea, 2-mercaptoethanol and Brij™ O20 were acquired from Carl Roth (GmbH and Co. KG, Karlsruhe, Germany). Sabouraud's dextrose 4% agar (peptone 5 g/L, tryptone 5 g/L, dextrose 40 g/L, agar 15 g/L) and disposable plastic microbiological labware were acquired from VWR (VWR, Milano, Italy).

2.2. Quantification of PS by UV – Vis spectroscopy

The concentration of **RB** was determined by ultraviolet–visible (UV–Vis) spectroscopy using a Tecan Spark microplate reader (Tecan Group AG, Männedorf, Switzerland) at an absorbance wavelength of 549 nm. Calibration curves were performed using phosphate-buffered saline pH 7.4 (PBS) over a concentration range of 0.5–25 μg/mL.

B-I$_2$ was synthesized following a synthetic procedure published elsewhere (Fedeli et al., 2015; Tricomi et al., 2025). Quantification of **B-I$_2$** was carried out by UV–Vis spectroscopy using a Tecan Spark microplate reader at 534 nm. Calibration curves were obtained using 96% ethanol over a PS concentration range of 1.5–50 μg/mL.

All calibration curves were generated from three independent dilution series (Fig. S1). Excel 2025 (Microsoft Corporation, Redmond, WA, USA) was used to perform a linear regression analysis of the absorbance–concentration relationship. According to the International Council for Harmonization (ICH) Guideline Q2 (R2) on the validation of analytical techniques, the slope of the calibration curve and the standard deviation of the response were used to compute the limits of detection (LOD) and quantification (LOQ) (ICH, 2023). The LOD and LOQ were 0.04 μg/mL and 0.13 μg/mL for **RB**, and 0.26 μg/mL and 0.80 μg/mL for **B-I2**, respectively.

2.3. Preparation and characterization of native BNC patches

The BNC was biosynthesized by *Komagataeibacter xylinus* (DSM 2325, German Collection of Microorganisms and Cell Cultures DSMZ, Braunschweig, Germany) as described previously (Beekmann et al., 2020) in Hestrin-Schramm medium (Hestrin and Schramm, 1954) at 28 °C and over seven days. The obtained fleeces were autoclaved (121 °C, 15 min, 2 bar; Systec GmbH & Co. KG, Linden, Germany) and washed by boiling in 0.1 M sodium hydroxide solution. After washing with double-distilled water until neutral pH was reached, circular patches were formed using a hollow punch (15 mm diameter; Boehm, La Fouillouse, France).

The BNC exhibited a dense, three-dimensional nanofibrous network, as visualized by scanning electron microscopy (SEM) (Fig. 2), with an average fiber diameter of 55 ± 9 nm and a mean pore size of 1.4 ± 0.5 μm. The molar mass of BNC produced by K. xylinus DSM 2325 under comparable conditions was reported in earlier studies measured by gel permeation chromatography coupled with a multi angle laser light scattering detector with a weight-average molecular weight of 1,300,000 g/mol and a polydispersity index of 1.17 [[Heydorn et al., 2023].

BNC specimens were stored in water to preserve their hydration. The hydration experiment was intended as a comparative screening method to evaluate differences between formulations. Only samples with intact shape and structure as well as macroscopically homogenous morphology were used. Diameter and thickness of the BNC samples were determined using a Profi caliper (PRECISE PS 7215, Burg-Wächter KG, Wetter, Germany), following the method described by Müller et al (Müller et al., 2013). Each BNC sample was measured at three different points and the arithmetic mean of the three measurements was taken as the height. The weight of the BNC samples was determined on an analytical balance (AT261 DeltaRange, Mettler Toledo Inc., Columbus, USA).

Microscopic characterization was performed by scanning electron microscopy (SEM) after lyophilization (VirTis GENESYS 25 EL 4, Biopharma Process Systems, Winchester, UK) at –30 °C and 0.011 bar. Cross-sections were sputtered (Hummer JR Techniques, Munich, Germany) with a thin film of gold–palladium at 5 kV and 5 mA for 90 s before visualization using a Carl Zeiss Gemini Ultra55 (Carl Zeiss AG, Oberkochen, Germany). Fiber diameter and pore size were determined by manual analysis of the obtained SEM micrographs using ImageJ 1.54p (Wayne Rasband, National Institutes of Health, MD, USA).

2.4. BNC patches loading

Two loading solutions were prepared to incorporate **RB** in BNC patches. In the first one, named *RB standard formulation*, **RB** was dissolved in PBS pH 7.4 at a concentration of 5 mg/mL. This concentration was selected for reasons of analytical convenience after release experiments through the nail. The second one, from now on *RB complemented formulation*, was prepared by dissolving glycerol (final concentration 75% w/w) in double-distilled water, followed by the addition of urea reaching a final concentration of 40% w/v. Finally, Rose Bengal was dissolved in this mixture to achieve a concentration of 5 mg/mL. The native BNC patches were then loaded by immersing each patch in 5.0 mL of their respective loading solutions in a dark glass vessel. The loading occurred under orbital shaking at 70 rpm for 48 h (IKA® KS 4000 control, IKA®-Werke GmbH & Co. KG, Staufen im Breisgau, Germany). **RB** was quantified spectrophotometrically. The incorporated amount was calculated from the concentration difference before and after loading, as previously described by Moritz et al (Moritz et al., 2014).

Two different loading solutions containing **B-I$_2$** were also prepared. A *B-I$_2$ standard solution* in which **B-I$_2$** was dissolved in propylene glycol at a concentration of 0.1 mg/mL and a final volume of 100 mL, and a *B-I$_2$ complemented solution* which was supplemented with urea (final concentration 20% w/v). Prior to the incorporation of **B-I$_2$**, native BNC patches were immersed in 5.0 mL of propylene glycol and subjected to orbital shaking at 70 rpm for 72 h to remove internal water, as previously described (Bellmann et al., 2023). This was to avoid the formation of drug aggregates or recrystallization due to the presence of water

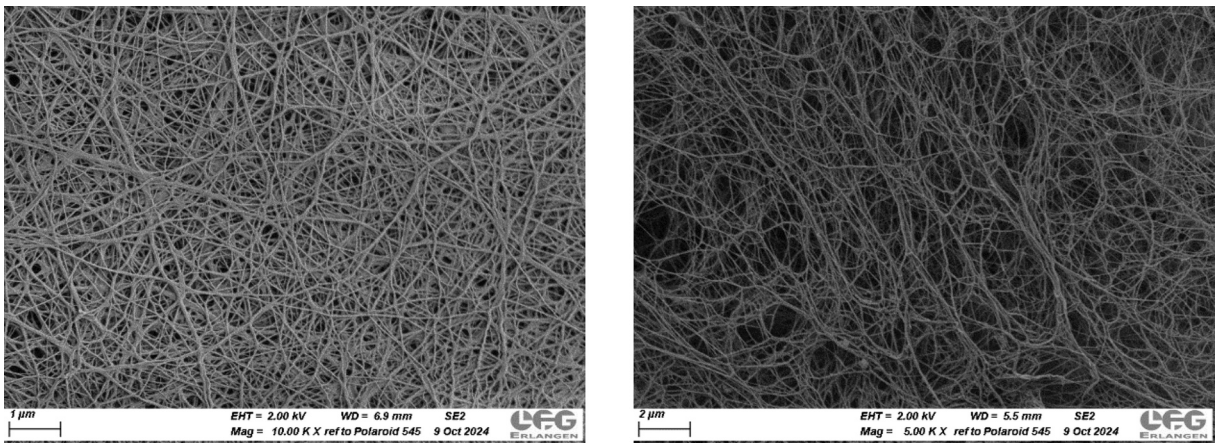

Fig. 2. SEM images of the surface (left) and the cross-section (right) of unloaded BNC produced by K. xylinus (DSM 2325) under static cultivation.

during the loading process (Fig. S2). The amount of loaded **B-I$_2$** was quantified as described for the loading of **RB**.

2.5. Transparency of the BNC patches

Transparency measurements were conducted using a Tecan Spark multiplate spectrophotometer (Karl et al., 2020). Native and loaded BNC patches were placed into 24-well plates (Greiner bio-one GmbH, Frickenhausen, Germany) and analyzed at 600 nm. For each BNC patch, the mean transmission from five equally distributed measurement points was expressed relative to the minimum detectable transmission. Experiments were performed in triplicate and repeated once.

2.6. BNC patches compression stability

The compression stability of both native and loaded BNC patches was assessed by measuring their weight and height before and after applying a 400 g weight for 10 min, following the method described by Alkhatib et al. (2017). Height of the patches was measured using a PRECISE PS 7215 calliper (Burg-Wächter KG, Wetter, Germany) (Hestrin and Schramm, 1954). Each patch was measured at three different positions, and the height was expressed as the mean of these measurements. Patch weight was determined using an analytical scale. Compressive strain (ε) was calculated as

$$\varepsilon = \frac{\Delta h}{h_0} * 100$$

where Δh is the reduction in height during compression and h_0 is the initial height.

Mass reduction (m_{Loss}) was calculated as

$$m_{Loss} = \frac{\Delta m}{m_0} * 100$$

where Δm represents the reduction in mass during compression and m_0 being the initial mass.

Experiments were performed in triplicates and repeated once.

2.7. Preparation of nail models

Keratin films were prepared from human hair, working as a model system for the human nail plate. Human hair was obtained from local volunteers. Onychomycosis heavily alters the nail plate (Hoy et al., 2012), increasing thickness and brittleness while disrupting the compact keratin matrix through fungal hyphae invasion. Although the human hair keratin-based film used here does not capture the full pathology of the disease, it serves as a highly reproducible and validated model sharing essential structural similarities with nail keratin (Lusiana et al., 2011). Their preparation largely followed the methodology described earlier (Bellmann et al., 2023,2022), with minor modifications. Human hair-derived keratin was selected to provide a standardized human keratin substrate, as our primary aim was to develop a model that more closely reflects the human nail. For this reason, a human-derived keratin source was considered more appropriate than animal-derived surrogate models for investigating the interaction of the formulation with human keratin. To extract keratin, 25 g of human hair, were incubated in 500 mL of Shindai solution (25 mM Tris, 2.6 M thiourea, 5 M urea, and 5% (v/v) 2-mercaptoethanol) for 72 h at 50 °C on an IKA orbital shaker running at 50 rpm, followed by filtration through filter paper and dialysis against deionized water for 72 h using a Spectra/Por® dialysis tube (6,000–8,000 Da; Spectrum Laboratories, Inc., Rancho Dominguez, Canada). After addition of glycerol (1% w/v final concentration) into the dialysate, 1 mL of the mixture was cast into a circular polytetrafluoroethylene mould with an inner diameter of 2 cm. The films were dried at 40 °C for 24 h. After the initial 4 h of drying, an additional 1 mL of dialysate was added to the moulds. Upon complete drying, the films received a final thermal treatment at 110 °C for 3 h. The thickness of the resulting films was precisely evaluated at their central region using an IP65 micrometre screw gaugeurea (Mitutoyo Corporation, Kawasaki, Japan). Only films free from visible imperfections, such as cracks or air bubbles, and possessing a uniform thickness between 120 and 160 µm, were utilized for experimental investigations.

2.8. Wetting capacity test of RB BNC patches

The two different RB BNC formulations were placed over dry nail models and stored at room temperature without cover under standard laboratory environmental conditions. The weight of the BNC patches and the nail models were evaluated after 0, 1, 2, 4, 6, 8 and 24 h on an analytical scale (Bellmann et al., 2022). The weight variations of the patches and nail models were divided by the density of the corresponding loading solution, which was determined through a pycnometric measurement at 20 °C, to calculate the volume of the fluid loss of the BNC patches and the fluid uptake of the keratin films. The percentage of fluid loss due to film moisturization (% Moist) was then calculated as

$$\%Moist = \frac{V_{uptake}}{V_{loss}} * 100$$

where V_{uptake} represents the fluid volume taken up by the keratin film and Vl_{oss} the fluid loss of the BNC patch. The percentage of fluid loss due to evaporation (*% Evap*) was calculated accordingly by Equation 4.

$$\%Evap = 100\% - \%Moist$$

The experiment was repeated under identical conditions, with the addition of OPSITE Flexifix® as a secondary dressing (Gupta et al., 2023). Data was analysed using the same equations.

Experiments were performed in triplicates and repeated once.

2.9. Drug release experiments using Franz diffusion cells

Release profiles of the loaded BNC patches were investigated using vertical Franz diffusion cells (Gauer Glas, Püttlingen, Germany) equipped with a 12.0 mL acceptor compartment and a diffusion area of 1.77 cm^2. The circular area connecting the donor and acceptor compartments has a diameter of 1,5 cm, resulting ina diffusion area of 1.77 cm^2.To minimize diffusion-limiting effects, patches were secured with a thin plastic cross, ensuring a direct contact area of 1.48 cm^2 between the patch surface and the release medium (Klemm et al., 2006). Different release media were chosen for each dye due to their different solubility. For **RB**, PBS pH 7.4 served as the release medium, while for **B-I_2** the release medium consisted of PBS pH 7.4 supplemented with 10% (v/v) ethanol and 6% (w/v) of the surfactant Brij™ O20 (polyoxyethylene (20) oleyl ether) (OECD, 2004). The freshly prepared, fully hydrated and loaded BNC patches with identical dimensions were positioned in the donor compartment and sealed with PARAFILM® to prevent water evaporation from the system. The acceptor compartment was filled with 12.0 mL of the release medium, maintained at 32 °C, and continuously stirred magnetically at 110 rpm throughout the experiment. Aliquots of 400 μL were collected at collected after 0, 0.25, 0.5, 1, 2, 4, 6, 8, 24 and 48 h and immediately replaced with an equal volume of prewarmed release medium to maintain a constant volume. The cumulative drug release was calculated by correcting for the drug removed during previous sampling. All experiments were performed in sink conditions, ensuring that the volume of the medium was large enough so that the solvent concentration never exceeded 10% of the saturation point. All experiments were conducted under light exclusion by wrapping the Franz diffusion cells in aluminium foil.

For permeation studies in the nail model, keratin films with homogenous thickness were selected and inserted between the donor and acceptor compartment, which were conducted using the same experimental setup as described before. The contact time and area to the acceptor medium were the same to ensure comparable conditions. The amount of residual drug within the keratin films after the permeation experiment was determined by extraction of the respective films for one week in 10 mL 96% ethanol followed by appropriate dilution with 96% ethanol and quantification method. Using the same procedure, the extraction was repeated with the addition of another 10 mL of ethanol 96% for another week. Experiments were performed in triplicates and independently repeated. The obtained data was used to calculate the percent of PS remaining in the nail model, after the release experiments and the percent that reached the donor compartment.

The overall amount of released drug was fitted to the Higuchi model (Higuchi, 1961), described by the following equation:

$$Q = \sqrt{Dt(2A - C_s)^*C_s}$$

where Q is the amount of drug released after time t per unit exposed area, D is the diffusivity of the drug in the homogeneous matrix media, A is the total amount of drug present in the matrix per unit volume, and Cs is the solubility of the drug in the matrix substance (Higuchi, 1963). The permeability coefficient P_{app} was evaluated by following equation reported by Bellmann et al. (2022).

$$P_{app} = \frac{dQ}{dt^*A^*c_0}$$

where dQ represents the amount of permeated drug within the time interval dt, A the area of the keratin film and c_0 the initial concentration of the drug in the donor compartment.

2.10. Photodynamic inhibition of Candida albicans

Sabouraud's dextrose 4% agar (SA) was prepared and autoclaved as *per* the manufacturer instructions. Then, 20 mL were dispensed in 9 cm petri dishes, cooled down until solidification and inverted. The petri dishes were left at room temperature for 24 h. Filter papers were cut and autoclaved beforehand. The nail models were hydrated (3 h in PBS with constant orbital stirring, 70 rpm) and pressed in between two sheets of paper embedded with milliQ water for 24 h, using two plates of glass as a press, ensuring that the nail models were flat at their placement. Upon utilisation, the nail models were passed through a 70% ethanol solution and PBS, and any humidity excess was removed using a sterile gaze. BNCs were removed from their respective loading solution and dried with a sterile gaze without further treatment. In the centre of a SA-dispensed 9 cm petri dish, it was placed either i) a filter paper circle (FP, 1.6 cm diameter), ii) a nail model with a FP on top, iii) a BNC or iv) a nail model with a BNC on top. After placing the dry FP, 100 μL of the PS-loading solutions used for their respective BNCs were transferred to the FP. The petri dishes were incubated 24 h at 37 °C, protected from the light and without stirring, letting the PS to diffuse into the SA.

Candida albicans ATCC 10231, was kept at −80 °C as a suspension in 30% glycerol and PBS. Typically, *C. albicans* was inoculated in Sabouraud's dextrose 4% agar and incubated at 30 °C for over 24 h. Then, 10 individual colonies were selected and dispersed in PBS, measuring its optical density at 600 nm (OD_{600}; Tecan 2000 Pro, Tecan Group AG, Männedorf, Switzerland) and diluting it to an OD_{600} of 0.25, corresponding roughly to 5×10^6 CFU/mL. The petri dishes with the diffused PS were recovered, and FP, BNC, and nails removed from them, keeping the BNC and the nails for further analysis. The petri dishes were photographed (Xiaomi, Redmi Note 14 Pro 5G) and then inoculated with the *C. albicans* suspension, using a cotton tip to spread the solution across the whole petri dish. The petri dishes were protected from environment light and designated plates to receive the light treatment were irradiated. A 528 nm laser (Necsel Green NovaLum, VHP) source was coupled into a multimode 500 μm core fibre and shaped via an optical lens, resulting in a circular irradiation spot of 6.4 cm in diameter. Laser power was measured with a calibrated power meter (Ophir Nova Display equipped with a PD300-UV-SH sensor head), obtaining a power output of 86 mW in the centre of the irradiation spot, and converted into irradiance by dividing it by the 1 cm^2 area of the detector, resulting in an irradiance of 86 mW/cm^2. Plates were exposed to a radiant exposure of approximately 31 J/cm^2, corresponding to an irradiation time of around 6 min per petri dish. Considering the chromosolvic absorption shifts when the PS are dissolved in the different loading solutions (Fig. S3), and calculating the light dose correction factor as described elsewhere (Schaberle, 2018) we obtained a corrected radiant exposure of around 20 J/cm^2 for RB and 30 J/cm^2 for B-I_2 (Table 1).

Irradiation was conducted at room temperature, with ambient illumination of the order of 1 μW cm^2 which was considered negligible with respect to the laser irradiance. After light irradiation, the petri dishes were incubated at 37 °C, photographing the plates at 24 and 48 h of post-light treatment against a dark background. Inhibition halos were obtained from the photographs, using ImageJ FIJI (Schindelin et al., 2012), and a macro script which can be found at Supplementary Material 2.

2.11. Statistical analysis

Statistical analysis was performed in MATLAB R2024b, through a One-way ANOVA, with an additional Tukey-Kramer's multiple comparison test. Significance in plots was expressed as ns: $p > 0.05$, *: $p < 0.05$, **: $p < 0.01$, ***: $p < 0.001$.

Table 1
Irradiation parameters per formulation.

Formulation	Irradiance	Uncorrected irradiation time	Uncorrected radiant exposure	Light dose correction factor	Corrected radiant exposure
RB	86 mW/cm^2	370 s	31.8 J/cm^2	0.7021	22.3 J/cm^2
RB with glycerol and urea	86 mW/cm^2	369 s	31.7 J/cm^2	0.5550	17.5 J/cm^2
B-I$_2$	86 mW/cm^2	392 s	33.7 J/cm^2	0.9075	30.6 J/cm^2
B-I$_2$ with PPG and urea	86 mW/cm^2	366 s	31.4 J/cm^2	0.9942	31.2 J/cm^2

3. Results and discussion

3.1. Preparation of the drug loaded BNC patches and characterization

RB and **B-I$_2$** were loaded into preassembled BNC patches, and the drug loading process was first assessed to optimize the release study (Moritz et al., 2014). To incorporate **RB** into BNC patches, two distinct loading solutions were employed (Table 1). The *RB standard formulation* contained **RB** dissolved in PBS, while the *RB complemented formulation* contained additionally urea and glycerol. The excellent water solubility of RB facilitated the preparation of loading solutions with high drug concentrations (5 mg/mL). Glycerol and urea were added to the *RB complemented formulation* based on previous work (Bellmann et al., 2022), which showed that 40% urea (w/v) in 75% glycerol and 25% water (w/w) was optimal for nail permeation of selected drugs, given the keratolytic effect of urea above 10% concentration (Celleno, 2018), while glycerol possess well-known moisturizing properties in topical formulations (Björklund et al., 2013; Chouhan and Saini, 2012).

B-I$_2$ remained insoluble under similar conditions as used for **RB**. For this reason, we chose propylene glycol as an optimal loading solvent due to its more hydrophobic characteristics and good biocompatibility. Like glycerol, it is widely recognized for significantly enhancing drug penetration in topical formulations (Carrer et al., 2020). Accordingly, two new distinct loading solutions were formulated for **B-I$_2$**: one containing **B-I$_2$** dissolved in propylene glycol (*B-I$_2$ standard formulation*), and the second supplemented with urea at 20% (w/v) (*B-I$_2$ complemented formulation*). The amount of urea corresponds to its saturation concentration. Nevertheless, under these conditions, the highest achievable concentration of **B-I$_2$** was 0.1 mg/mL (Table 2).

Under the chosen experimental conditions, the loading efficiency was expected to be approximately 20%, dependent on the volume ratio of BNC to loading solution (Karl et al., 2020; Wiegand et al., 2015). The loading efficiency for **RB** was found to be 19.5 ± 1.7% and 19.1 ± 2.5%, for *RB standard* and *RB complemented formulation* respectively, while for **B-I$_2$** it reached 21.0 ± 2.7% and 25.5 ± 6.2% in the *standard* and *complemented formulations* respectively (Fig. 3). All loaded patches exhibited a homogeneous appearance, with no visible drug aggregates, recrystallization or any other macroscopically visible changes.

3.2. Physical characterization of the BNC patches

For pharmaceutical devices, robust mechanical stress resistance is essential during production, storage, transport and handling. This directly contributes to the product's longevity and stability over time, ultimately enhancing patient compliance. The mass reduction (Fig. 4a) and the compressive strain (Fig. 4b) of the PS-loaded BNC patches were compared with the native BNCs, which typically show a mass reduction of 64% and a compressive strain of 71%. It was found that the loading of **RB** solutions did not affect the physical characteristics, observing a mass

Table 2
Composition of the different loading solutions used in this work.

Standard formulation	Complemented formulation
RB 5 mg/mL in PBS	**RB** 5 mg/mL, 75% glycerol (w/w) and urea 40% (w/v)
B-I$_2$ 0.1 mg/mL in propylene glycol	**B-I$_2$** 0.1 mg/mL in propylene glycol and urea 20% (w/v)

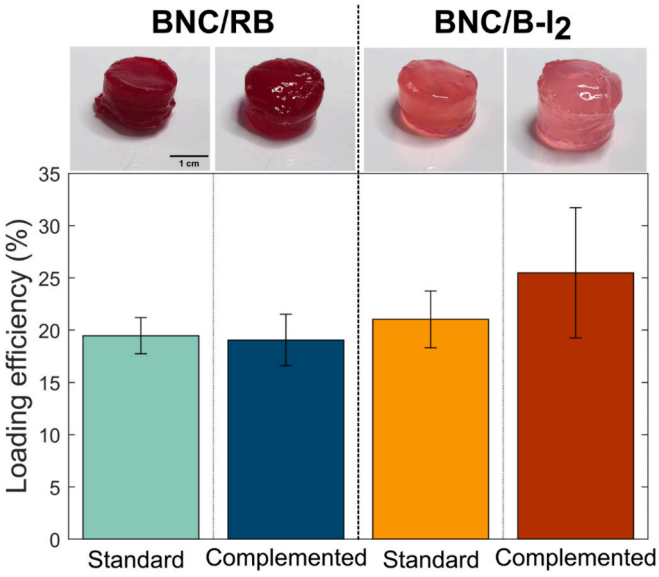

Fig. 3. Loading efficiency, expressed as a percentage relative to the amount of PS present in the loading solution, evaluated as reported in the section: *BNC patches loading*. On the top of the graph, representative photos of the BNC obtained patches. Loading efficiency results are expressed as mean ± SD of 6 different patches from two independent experiments.

reduction of around 65% and a percent of compressive strain of around 73% (Alkhatib et al., 2017; Bellmann et al., 2022). Meanwhile, the addition of **B-I$_2$** solutions, and the subsequent substitution of water with propylene glycol, decreased the mass reduction (50%) and the compressive strain (56%). Remarkably, changes in mass reduction and compressive strain were not found between the standard and the urea-complemented formulations, for both types of PS-loaded BNC patches, which coincides with previous reports (Alkhatib et al., 2017; Karl et al., 2020) where the presence of urea did not affect the physical properties of the BNC patches.

Transparency is a crucial physicochemical characteristic for medical patches, as it serves two main purposes. First, it allows for the assessment of disease progression over time without the need to remove the device, enabling doctors to perform non-invasive inspection of the nail bed, which is clinically highly advantageous. Second, transparency could potentially play a vital role in PDT by ensuring the transmission of light through the material for drug activation. According to standard transparency test methods (D20 Committee, n.d.; Zhao et al., 2022) a wavelength of 600 nm was selected to avoid interference from absorption by either the incorporated PS or the BNC matrix. Consequently, the measured signal is mainly affected by light scattering from the BNC network rather than absorption (Fig. 4c). For the BNC matrix effects can be excluded as already seen in several publications before (Aigaje et al., 2023; Karl et al., 2020; Yudianti et al., 2016). In preliminary experiments, measuring the drug dissolutions confirmed that both PS did not interfere with the signals at 600 nm (Fig. S3).

Our results show that transparency is influenced by the addition of glycerol and propylene glycol during the PS loading, when compared with the native BNC patches. **RB**-loading decreases light transmission

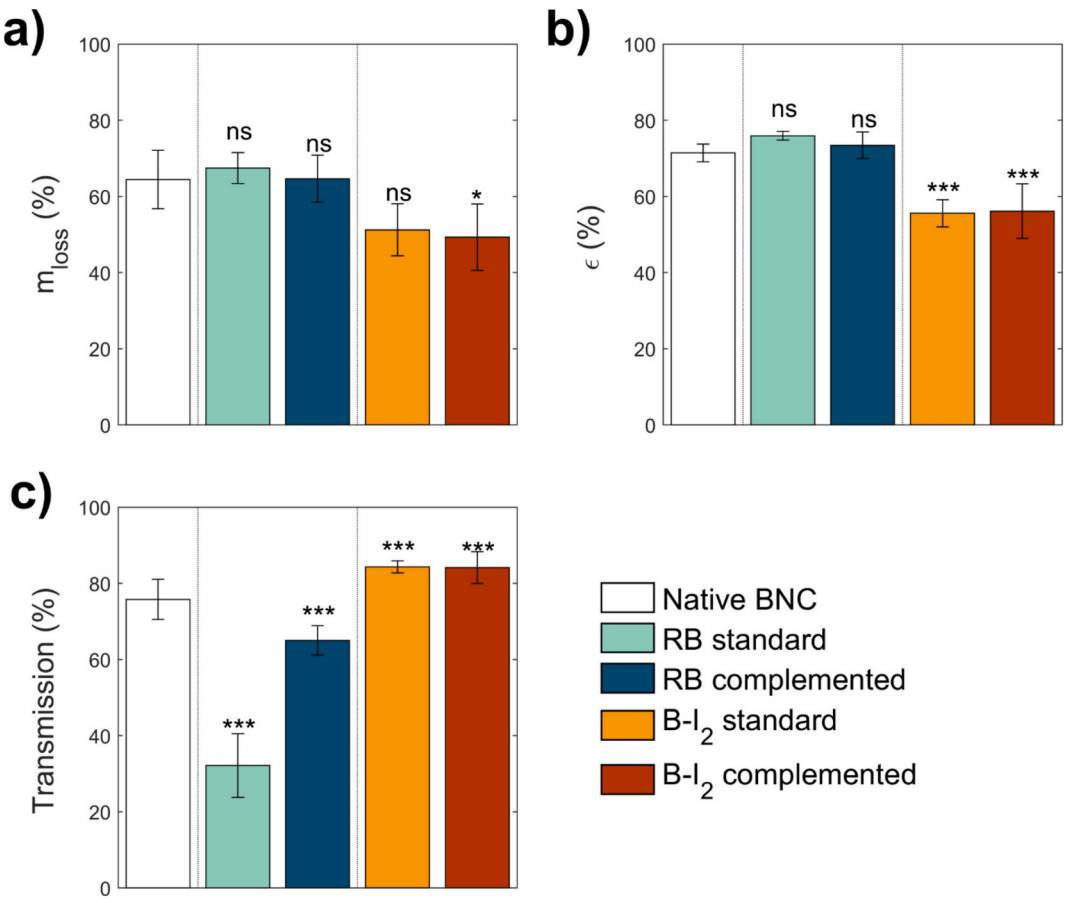

Fig. 4. Physicochemical properties of BNC patches. a) Percent of mass loss and b) percent of compressive strain (ε) determined after compression with a 400 g weight for 10 min. Results are expressed as mean ± SD for 6 different patches from two independent experiments. c) Transparency of BNC patches expressed as percent of transmitted light at 600 nm, determined through UV–vis spectrometry. Values were obtained from 5 equally distributed points per patch and are presented as mean ± SD for 6 different patches from two independent experiments. The obtained data was analysed through a One-way ANOVA, with an additional Tukey-Kramer's multiple comparison test; comparison with the native BNCs, ns: $p > 0.05$, *: $p < 0.05$, **: $p < 0.01$, ***: $p < 0.001$.

with respect to the native BNC patches, while the introduction of glycerol significantly recovered their transparency, from 32.2 ± 8.4 to 65.0 ± 3.9% (One-way ANOVA, $p < 0.001$ Tukey-Kramer's multiple comparison test), (Fig. 4c) but without reaching the transparency of the native BNCs 75.8 ± 5.3%. This can be explained by a reduction of the ratio between the refractive indices of the cellulose network and the absorbed solvent, resulting in a diminished light scattering. Glycerol has a higher refractive index than water, which matches better with the matrix. This leads to a higher visual transparency depended on the amount of incorporated glycerol (Wildner and Drummer, 2019). Interestingly, the addition of propylene glycol for the **B-I$_2$**-loaded patches resulted in a higher transparency, with respect to the native patches, although no further additive effect is observed comparing the standard (84.3 ± 1.6%) and complemented formulations (84.1 ± 4.2%).

3.3. Wetting capacity of RB BNC patches

One important parameter that our study needed to consider is the capacity of transferal of the loading solution from the BNC into the nail plate, thus for downstream applications we decided to use a hair keratin nail plate model. The limited availability and the biological variability of human and animal nail plates for drug permeation studies has prompted the use of a nail plate model based on human hair keratin, prepared according to the method described by Lusiana et al. (2011). In addition to the ready availability of the source material, the extraction and film-forming process enables the production of multiple keratin films with highly consistent composition and thickness, facilitating large-scale permeation studies with reproducible film quality. This approach minimizes biological variability between samples and allows the parallel evaluation of numerous formulations under standardized experimental conditions. Although the chosen nail model cannot fully reproduce the physiological properties of native nail tissue, its comparatively low water absorption capacity suggests that the hydration potential of the BNC patches is more likely to be underestimated than overestimated in the present model compared to in vivo nails. Lusiana et al. demonstrated that human keratin hair films reproduce the permeation behavior of keratinous nail tissue reasonably well and proposed this model as a suitable screening tool for ungual drug delivery studies (Lusiana et al., 2011). This applies particularly to hydrophilic compounds such as RB, whereas lipophilic compounds may permeate more readily through keratin films than through bovine hoof or human nail.

The two RB patch formulations featured distinct water contents, in contrast to the entirely anhydrous **B-I$_2$** systems. This allowed for an evaluation of how varying water-to-glycerol ratios within the BNC matrix influenced the wetting capacity upon contact with the nail model. To account for environmental factors, these assessments were conducted both with and without **OPSITE Flexifix®** coverage, specifically to isolate the impact of evaporation. **RB** patches were prioritized for this study as their aqueous nature enables a direct investigation of the interplay between hydration and evaporation, a mechanistic dynamic absent in the anhydrous **B-I$_2$** formulations. The wetting capacity of BNC patches loaded with **RB** was evaluated on nail models with a homogeneous thickness of 152 ± 4 µm. The wetting capacity initially was

assessed based on weight variations of both the patches and the nail models without coverage. To express this data as transferred volume, it was necessary to take in account the density of the incorporated fluids, determined through a pycnometer: **RB** in PBS had a density value of 1.01 g/mL while RB with 40% urea and 75% glycerol had a density value of 1.20 g/mL. As previously reported (Bellmann et al., 2022), the presence of glycerol was found to improve the wetting capacity of BNC patches over the investigation period. The wetting capacity illustrated in Fig. 5 provides a quantitative assessment of the fluid transfer dynamics between the BNC patches and the nail model. In the absence of an occlusive cover (dashed lines), both formulations showed a limited moisturizing effect due to rapid and competitive environmental evaporation. The **standard RB patches** (circles) reached a negligible peak of 0.01 mL before returning to the nail's baseline mass within 4 h, showing a total loss of hydration. In contrast, the **complemented** patches (squares) maintained a significantly higher profile, reaching a peak volume of approximately 0.035 mL between 2 and 4 h, more than triple than the standard formulation. Although this volume gradually declined, the **complemented** patches sustained a residual hydration of 0.03 mL at 8 h and 0.015 mL after 24 h, confirming a superior, yet still vulnerable, primary hydration capacity. However, a good shift was observed under occlusive conditions (solid lines). The use of the **OPSITE Flexifix®** cover effectively reduced water evaporation, allowing the internal composition of the patches to dictate the wetting performance. The **standard** formulation under cover peaked at 0.055 mL, but its effect diminished after 8 h. In contrast, the **complemented** formulation exhibited a significantly superior and sustained wetting profile: it reached a maximum transferred volume of 0.091 mL at 4 h and remained remarkably stable, preserving a volume of 0.065 mL even at the 48-hour mark (data not shown). These values demonstrate that the high glycerol content not only enhances the initial fluid delivery but also creates a long-lasting hydration reservoir when paired with an occlusive dressing.

3.4. Drug release experiments using Franz cells

The release of **RB** and **B-I$_2$** was investigated using Franz vertical diffusion cells, to achieve a unidirectional, direct contact of the BNC to the release medium under sink conditions. Given **RB**'s high water-solubility, it allowed for effective drug diffusion and release from the BNC patches, showing a cumulative release profile in both RB

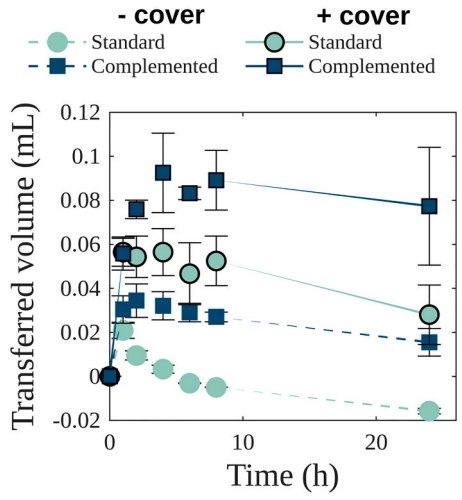

Fig. 5. Transferred volumes (mL) from BNCs loaded with **RB** without (circles, light blue) or with urea (squares, dark blue). The efficiency of the transfer was evaluated over time, in the absence (dashed lines) or the presence (solid lines) of a polymer cover. Data is expressed as the mean ± SD from two individual experiments, with 3 patches per condition.

formulations, with a fast release in the first 8 h (ca. 50%), followed by a slower release up to 24 h (ca. 70%) and a plateau for both the standard and the complemented formulation (Fig. 6a). After 24 h, the release rate is reduced, until it reaches a plateau after 72 h at 90 ± 9% and 75 ± 10% for the standard and complemented formulations, respectively. The decline in release rate observed after 24 h can be attributed to the reduction of the concentration gradient between formulation and release medium, accompanied by an increasing diffusion distance from deeper regions of the BNC patch. Finally, it can be observed that the higher density of the complemented formulation, which is attributable to the presence of glycerol, had a limited influence on the diffusion rate of the drug.

B-I$_2$ was selected as a lipophilic photosensitizer, contrasting the hydrophilic Rose Bengal, due to its small molecular size, which minimizes steric hindrance across the nail's molecular sieve (Elsayed, 2015; Gupta et al., 2023). Furthermore, while the healthy nail plate is predominantly hydrophilic, it incorporates lipid pathways: during onychomycosis, this structural network is disrupted and remodeled by fungal hyphae (Malallah et al., 2024). A lipophilic agent like B-I$_2$ is therefore highly suitable to evaluate drug partitioning into these compromised, fungus-colonized domains since transungual permeation is governed by a multifactorial combination of properties, including molecular size, lipophilicity, hydrophilicity, keratin affinity, ionization state, and formulation characteristics (Gupta et al., 2023).

Due to its low solubility in aqueous media and to guarantee the full solubility of the dye, for **B-I$_2$** we changed the release medium in the Franz vertical cell from PBS pH 7.4 solution to PBS supplemented with 10% (v/v) ethanol and 6% (w/v) of the surfactant Brij™ O20 (OECD, 2004). Under these conditions, we found for **B-I$_2$** a comparable release profile. In this case, a faster initial release rate was demonstrated reaching 14 ± 4% after 8 h, followed by a slower release rate with a lower release of **BI$_2$** reaching a plateau after 72 h (24 ± 8%). The slow release and lower equilibrium percentages were attributed to the different drug solubility and high viscosity of propylene glycol, which was used as the loading solution for **B-I$_2$** (Fig. 6b). Due to the limited amount of urea contained in the complemented solution of **B-I$_2$**, its release was not analysed.

To investigate the release mechanisms of PSs from BNC patches, the cumulative release profiles were fitted to several commonly employed kinetic models, such as Higuchi, first order and zero order release models. The comparison of the R^2 analysis revealed that the Higuchi model provided the highest fit for the release data (Supplementary Material 3). Consequently, the results adhere to the law described in Equation 5 (see above). This adherence to the Higuchi model suggests that the dominant mechanism for the release of the tested drugs from BNC patches is Fickian diffusion, where drug movement from the matrix is primarily controlled by the concentration gradient and is proportional to the square root of time (Higuchi, 1961). The inherent network structure of BNC is intrinsically suited to support such a diffusive process (Huang and Brazel, 2001; Siepmann and Siepmann, 2012).

3.5. Nail permeation of photosensitizers

The permeation of **PSs** from BNC patches through the nail model was evaluated for the different formulations, by adding the nail model between the patch and the Franz cell. The BNC patches were positioned in the donor compartment and sealed with PARAFILM®, just as described for the experiments without the nail model. For standard **RB** formulations (Fig. 7a), around 4.0 ± 1.6% of the drug passed through the nail model after 24 h, showing a decrease of 73% with respect to the nail-less conditions. On the other hand, the complemented formulation showed an enhanced permeation, resulting in 11.5 ± 1.2% permeation at 24 h. Equilibrium for these two formulations was reached at 48 h, with 4.0 ± 0.3% and 12 ± 3% drug release, respectively. Conversely, for BNC patches containing **B-I$_2$** (Fig. 7b), 15 ± 2. % drug passed through the nail model after 24 h for the standard formulation, while the complemented

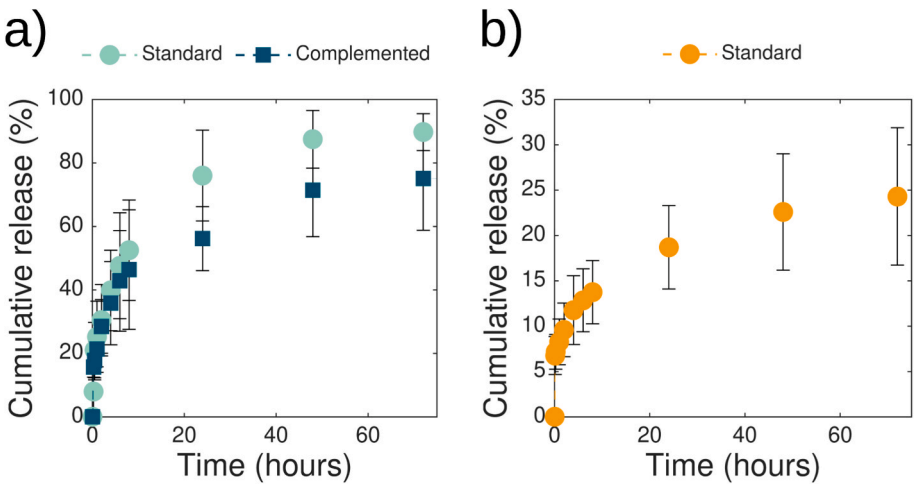

Fig. 6. Cumulative release from the BNC of (a) **RB** and (b) **B-I$_2$** determined *via* UV–vis spectrophotometry. The release was assessed in a Franz diffusion cell at 32 °C, in PBS (a) or in 6% w/v Brij® O20, 10% v/v ethanol PBS solution (b) as the release media. Results are expressed as mean ± SD from two independent experiments, with 3 BNC patches each.

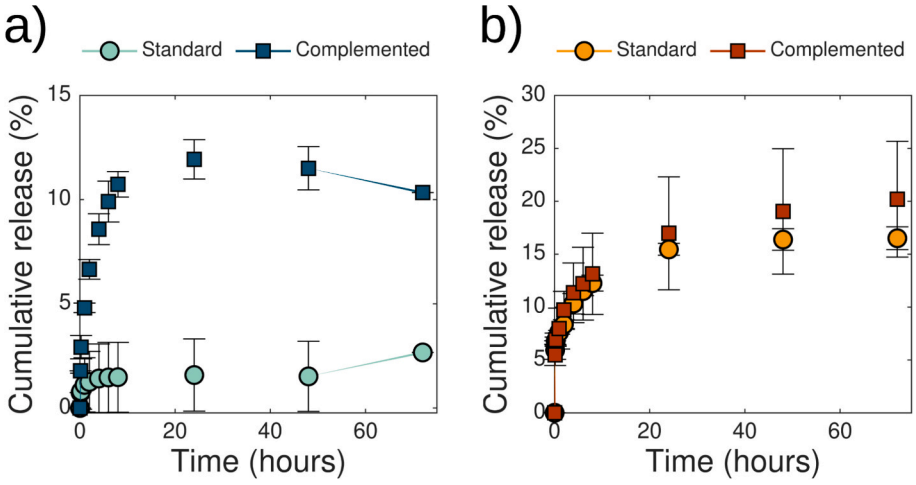

Fig. 7. Cumulative release from the BNCs of (a) **RB** and (b) **B-I$_2$**, when passing through the nail model, determined *via* UV–vis spectrophotometry. The release was assessed in a Franz diffusion cell at 32 °C, in PBS (a) or in 6% w/v Brij® O20, 10% v/v ethanol PBS solution (b) as the release media, with the nail model placed between the BNC and the Franz diffusion cell. Results are expressed as mean ± SD from two independent experiments, with 3 BNC patches each.

formulation delivered up to 18 ± 2%. In this case, the equilibrium was reached at cumulative drug release values of 16.5 ± 1.1% and 20 ± 5% after 72 h, respectively.

All experiments were repeated independently and showed reproducible results. Regarding hydration, all permeation experiments were performed using freshly prepared, fully hydrated BNC patches with identical dimensions and loading. The keratin films were always prepared following the same protocol and selected only when showing homogeneous dimensions. The contact time and area to the acceptor medium was the same to ensure comparable hydration of the nail models. All donor compartments were sealed with Parafilm® to prevent water evaporation during the experiments and to accomplish comparable hydration states. The reliability of the Franz cell setup was validated by Rose Bengal, whose delivery dropped from 75% to 12% across the keratin barrier, confirming the system discriminates between carrier release and true transungual transport. For the lipophilic **B-I$_2$**, adding 10% ethanol and 6% Brij O20 to the receptor phase maintained the sink conditions required for Higuchi kinetic modeling.

Although these additives might slightly alter the barrier properties, meaning absolute **B-I$_2$** permeation rates reflect these specific setup conditions rather than a direct comparison to Rose Bengal, they ensure a perfectly valid internal comparison between the two **B-I$_2$** formulations tested under identical parameters.

The apparent permeability coefficient (P_{app}), calculated at 48 h according to Equation 6, demonstrated that supplementation of the formulation with urea enhanced the permeation of the photosensitizers through the nail model (Fig. 8a). Considering the **RB** formulations, the addition of glycerol and urea increased the mean permeation coefficient from $2.7 \pm 1.2 * 10^{-7}$ cm/s to $1.5 \pm 0.8 * 10^{-6}$ cm/s, demonstrating that the presence of urea improved the permeation of **RB**. Comparable values, in the same order of magnitude as this latter data, were obtained using BNC patches containing **B-I$_2$**, yielding $1.7 \pm 0.5 * 10^{-6}$ cm/s and $2.3 \pm 0.9 * 10^{-6}$ cm/s for the standard and complemented formulations, respectively.

According to Täuber and Müller-Goymann (2015), diffusion of drugs through the nail model depends on various factors, including the physicochemical properties of the drug itself, the formulation composition, the structural and chemical characteristics of the keratin film, and the experimental conditions such as hydration and temperature. Due to the poor aqueous solubility of **B-I$_2$**, the acceptor medium had to be supplemented with 10% ethanol and 6% Brij O20 to maintain sink conditions. Ethanol can act as permeation enhancer in nail drug delivery

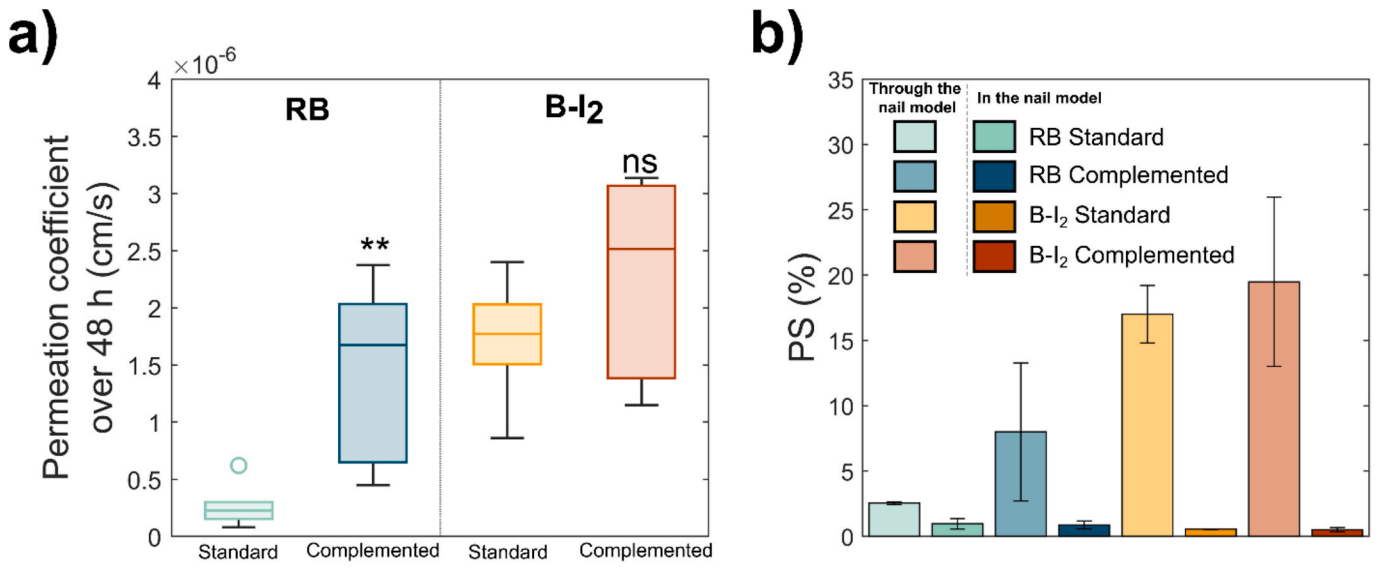

Fig. 8. (a) Permeability coefficient of **RB** and **B-I$_2$** drugs through the nail model over 48 h. Results are expressed as box charts, obtained from 6 individual patches from two different experiments. Permeability coefficients were compared using a paired-sample *t*-test; ns: non-significant, **: $p < 0.01$. (b) Percentage of drug permeated through the nail model (left stacked bars) and remained in the nail model (right stacked bars). Results are expressed as mean ± SD from 6 individual patches from two independent experiments. Permeability coefficients were compared using a paired-sample *t*-test; no significant differences were found between the standard and the complemented formulations.

by increasing drug solubility and facilitating diffusion through the keratin network, but moderate concentrations (20% v/v) have been reported not to induce relevant swelling of nail samples (Vejnovic et al., 2010). Consequently, the absolute permeation coefficients determined for **B-I$_2$** should be interpreted as specific values obtained under the selected sink conditions rather than as directly comparable to those determined for **RB**. Importantly, this limitation does not affect the comparison between the two **B-I$_2$** formulations, since both were evaluated under identical experimental conditions.

Subsequent to the release experiments, the extraction of residual drug from the nail model facilitated the evaluation of drug distribution at equilibrium. No relevant differences were observed in the percentage of residual drug extracted from the nail in either scenario, regardless of the formulation type. However, these additives demonstrated a notable impact on the varying quantities of the two drugs that successfully transited through the nail (Fig. 8b).

3.6. Photodynamic antifungal activity

The photodynamic antimycotic activity of the PSs released from the BNCs, in the presence and absence of the nail model were investigated. As best of our knowledge, this is the first attempt to evaluate the photodynamic effect of released **RB** and a **B-I$_2$** compound. We evaluated the capacity of the photosensitizers to permeate in the Sabouraud's agar (SA) media, followed by their capacity to inhibit the growth of *Candida albicans* ATCC 10231 after light exposure (Fig. S4). An ideal photosensitizer lacks toxicity in the dark, but this is concentration-dependent and it is not unusual to find that photosensitizers at high concentrations become toxic (Baglo et al., 2020; Eckl et al., 2018). To assess this, we consider the photodynamic inhibition as the difference between the light and dark inhibition areas, comparing the obtained effect when delivering a known concentration of the PSs through a filter paper (FP), or through the BNC, with and without the nail in between the BNC and the SA media (Fig. 9). The presence of the FP condition is vital to understand the intrinsic effects of the PS and the loading solution, with and without light irradiation, as under this condition we have a simplified loading solution transfer from a plain surface into the agar, without considering the diffusion of the loading solution within the BNC. Additionally, this condition demonstrated that the presence of limited volumes of the loading solutions were not toxic to the growth of *C. albicans* in the absence of light (Fig. S4), which contrasts with the scenario of the BNCs, where in the absence of light an inhibition effect was observed, likely due to high concentrations of the diverse components of the loading solution.

We found that when delivering **RB** through a filter paper (Fig. 9a), the presence of the nail decreased the photodynamic inhibition from 14.3 ± 0.2 to 3 ± 4 cm^2, while when delivering RB through a BNC, the presence of the nail decreased the photodynamic efficiency from 17.2 ± 1.7 to 7 ± 10 cm^2, although when compared, the photodynamic inhibition when delivering **RB** through the nail with a BNC was still increased when compared with the filter paper. The addition of urea to the formulation increased the photodynamic inhibition whenever the nail was present, but no significant improvement was observed when the nail was absent (Supplementary Material 3, Table S16). The keratinolytic effect of urea rescues the photodynamic inhibition, obtaining values similar to those observed in the absence of the nail.

For the case of **B-I$_2$**, we observed low photodynamic inhibition areas and no differences in the presence of the nails or in the presence of urea (Fig. 9b). Remarkably, the presence of the BNCs loaded with **B-I$_2$** was enough to produce an inhibition halo, even in the absence of light irradiation, an effect that could be related to the diffusion, osmotic effects and/or intrinsic toxicity of propylene glycol (Kinnunen and Koskela, 1991). We observe that **B-I$_2$** does not diffuse into the agar, limiting a potential photodynamic effect to the immediate region where **B-I$_2$** was placed on the agar. Nevertheless modest, **B-I$_2$** showed a photodynamic activity when using low loading solution volumes.

These preliminary results indicate the likeliness of our formulation to deliver PS molecules, preserving their photodynamic properties. It would be ideal that the PS delivered results toxic only upon light irradiation, allowing a tight control on the triggering of the photodynamic effect.

Given the low applied dose and limited transungual permeation, topical delivery of both PS is expected to result in minimal systemic exposure. Furthermore, their therapeutic activity is strictly dependent on local light activation. In the absence of irradiation, the PS remain photochemically inactive and do not generate ROS. Because light exposure is confined strictly to the infected nail tissue, the risk of clinically relevant systemic adverse effects is considered unlikely. Phase II

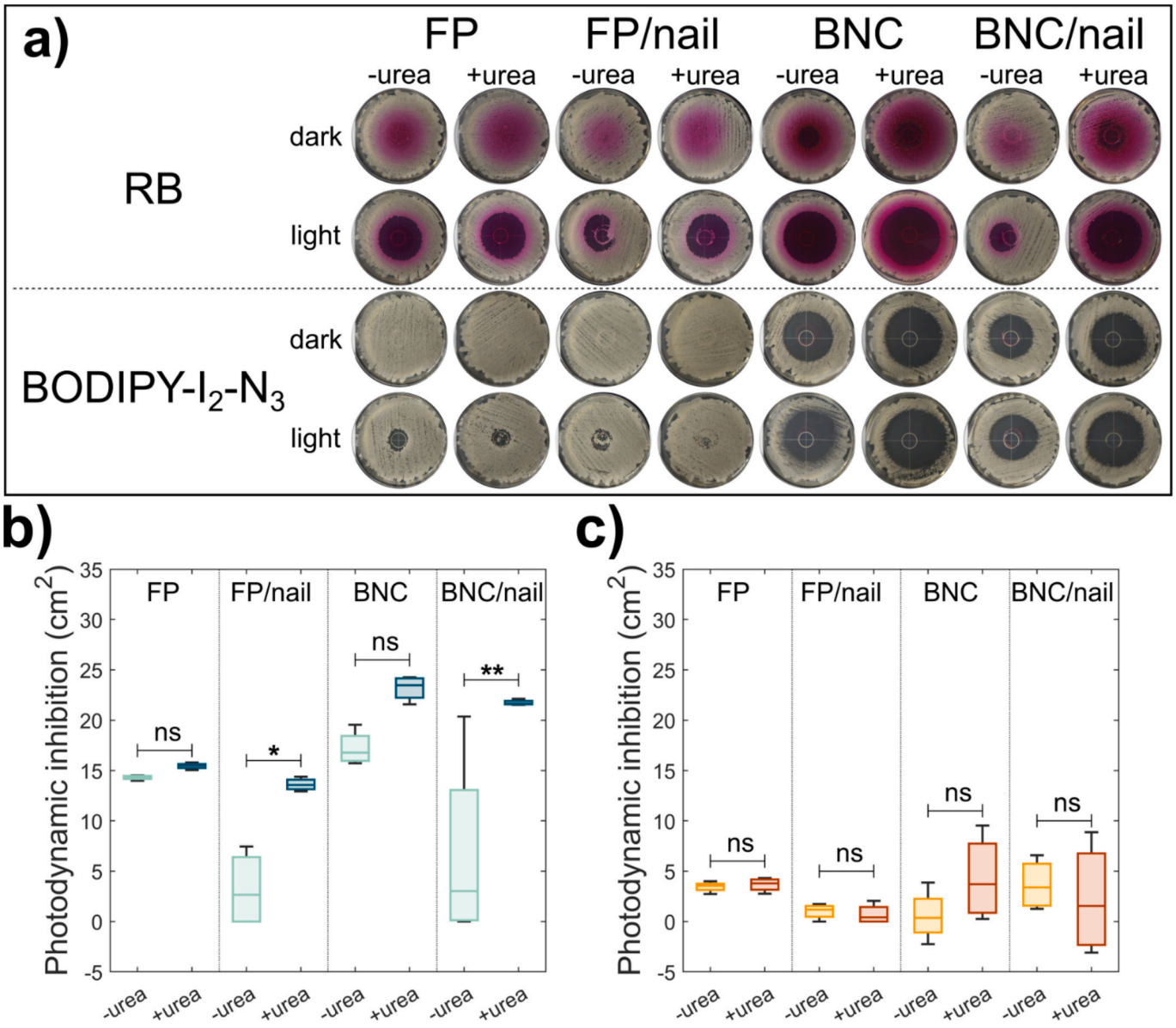

Fig. 9. Inhibition of *C. albicans* ATCC 10231 growth, when in presence of **RB** and **B-I$_2$** diffused in SA media, in the absence or presence of light irradiation (a). PSs were delivered into the SA media through a filter paper loaded with 100 μL of loading solution (FP), a filter paper loaded with 100 μL of loading solution through a nail (FP/nail), a BNC or a BNC through a nail (BNC/nail), in the absence or presence of urea. Photodynamic inhibition of **RB** (b) and **B-I$_2$** (c), considered as the difference between the light and dark inhibition areas. Results shown are four technical replicates of a single experiment. The obtained data was analysed through a One-way ANOVA, with an additional Tukey-Kramer's multiple comparison test; ns: $p > 0.05$, *: $p < 0.05$, **: $p < 0.01$, ***: $p < 0.001$.

clinical studies with intralesional RB (Thompson et al., 2015; Wachter et al., 2003), where substantially higher doses of RB are administered directly into tumours, demonstrated that systemic toxicity is minimal and adverse events are predominantly confined to the application site. Pharmacokinetic analyses further showed prolonged retention of RB at the application site, with only limited systemic exposure.

Onychomycosis heavily alters the nail plate, increasing thickness and brittleness while disrupting the compact keratin matrix through fungal hyphae invasion (Hoy et al., 2012). These changes can affect the barrier properties of the nail and consequently influence the diffusion and penetration of topical compounds (De Monte Vidal et al., 2026). Although the human hair keratin-based film used here does not capture the full pathology of the disease, it serves as a highly reproducible and validated model sharing essential structural similarities with nail keratin (Lusiana et al., 2011). Compared to conventional locally applied therapeutic options like nail lacquers, creams, and solutions, the proposed BNC patches offer several advantages. The patches are easy to apply and demonstrate a high transparency which allows a continuous inspection of the nails and the therapeutic progress. In dependency of the water content of BNC even a sticky behavior towards flat surfaces was noted (Bellmann et al., 2022). While medicated nail lacquers primarily rely on solvent evaporation to form a drug-containing film on the nail surface, the hydrated BNC matrix acts as a reservoir that continuously supports moisture to the nail. Increased nail hydration is known to enhance nail permeability by swelling the keratin network, thereby facilitating drug transport. This effect was further supported by the incorporation of urea and glycerol. In earlier studies, for ciclopirox-loaded BNC, an enhanced permeation of the drug from the BNC patches could be observed compared to the commercial Ciclopoli® lacquer (Bellmann et al., 2022). Unlike conventional delivery systems, which rely solely on continuous drug exposure, the proposed system enables spatially and temporally controlled activation of the PS by light that may reduce undesired off-

target effects. The use of photosensitizing molecules has the additional advantage that the PS act as a pro-drug, as they are not the molecules exerting the biological effect, with short-lived reactive oxygen species being responsible for an extensive and unspecific microbial damage, to which cells cannot react or produce resistance (Maldonado-Carmona et al., 2020). Finally, the BNC-based technology offers significant advantages from an environmental perspective. BNC is characterized by a resource-efficient manufacturing process carried out under mild conditions that produces a material with high purity, so that less complex purification processes are required. Furthermore, BNC can be produced from waste materials and industrial byproducts (Liu et al., 2023), thereby supporting resource-efficient, circular production. The BNC material *per se* favors a major advantage over conventional delivery systems as it is sustainable, renewable, and biodegradable, providing an environmentally friendly alternative to synthetic polymer-based delivery systems.

Overall, the light-activated BNC-based patches combine patient-centered drug development with environmental sustainability, a responsible use of antimicrobial strategies and have the potential, as an innovative technology platform, to contribute to a sustainable healthcare system.

4. Conclusions

The use of BNC patches was analysed as a suitable delivery system for photosensitizers in the photodynamic treatment of onychomycosis. The patches were robust and efficient with high capacity of PS adsorption. The use of two different PS molecules, **RB** and **B-I$_2$**, with different aqueous solubilities, imposed the choice of different solvent formulations that could guarantee the absence of aggregation inside the patches. Both formulations were able to dissolve important amounts of urea, whose keratolytic effect revealed an important effect in permeation studies across nail models at the vertical Franz cells analysis. This afforded the preliminary data that allowed the preparation for *in vitro* studies performed on a model strain of *C. albicans*. Our results indicate the effectiveness of our formulation to deliver PS molecules, preserving the photodynamic properties of the PS. Our analytical and microbiological experimental evidence supports the idea that the presence of urea in nail-targeted formulations allows for a more efficient delivery of drugs into the nail, bypassing the low permeability of the nail. The evaluation of the PDT effect of **B-I$_2$** was limited by the toxicity related to the high concentration of propylene glycol and to the low diffusion of **B-I$_2$** through the agar. However, it is of interest to extend these studies to the use of hardly-water-soluble molecules to extend the number of efficient PS available for this promising approach.

In perspective, further studies should test the developed BNC-based delivery systems for PDT for their capacity to induce light-driven death in more challenging conditions, such as hypoxia, diverse nail plate structure (i.e. brittle nail with increased desiccation), presence of pigmentation, while also taking in consideration the use of other pathogenic models, such as *Trichophyton rubrum*. The current study is the fundamental stone for further research with high translational potential, combining drug release and light-driven strategies for the treatment of fungal diseases.

CRediT authorship contribution statement

Francesca Mancusi: Writing – original draft, Investigation. **Mara Wesinger:** Writing – review & editing, Writing – original draft, Investigation. **Nidia Maldonado-Carmona:** Writing – review & editing, Writing – original draft, Methodology, Investigation, Data curation. **Elisa Bianchi:** Writing – review & editing, Investigation. **Giacomo Insero:** Writing – review & editing, Writing – original draft, Resources, Investigation. **Giovanni Romano:** Writing – review & editing, Resources, Investigation, Data curation. **Barbara Richichi:** Writing – review & editing, Writing – original draft, Supervision, Methodology. **Stefano Cicchi:** Writing – original draft, Supervision, Funding acquisition. **Dagmar Fischer:** Writing – review & editing, Writing – original draft, Supervision, Conceptualization.

Declaration of competing interest

The authors declare the following financial interests/personal relationships which may be considered as potential competing interests: Stefano Cicchi reports financial support was provided by NextGenerationEU. If there are other authors, they declare that they have no known competing financial interests or personal relationships that could have appeared to influence the work reported in this paper.

Acknowledgements

FM and SC thank Prof. Fischer and her research group for their hospitality, valuable discussions, and support during the research stay. Special thanks are due to Andreas Dzierza for his voluntary contribution and for providing the hair samples used in the experimental procedures. NM-C, GI and GR thank Simona Pollini for her technical help.

This work was supported by the European Union under the NextGenerationEU project ECS00000017 "Ecosistema dell'Innovazione" Tuscany Health Ecosystem (THE, PNRR, Spoke 4: Nanotechnologies for diagnosis and therapy).

Appendix A. Supplementary data

Supplementary data to this article can be found online at https://doi.org/10.1016/j.ijpharm.2026.127299.

Data availability

Data will be made available on request.

References

Agazzi, M.L., Ballatore, M.B., Durantini, A.M., Durantini, E.N., Tomé, A.C., 2019. BODIPYs in antitumoral and antimicrobial photodynamic therapy: an integrating review. J Photochem Photobiol C: Photochem Rev. 40, 21–48. https://doi.org/10.1016/j.jphotochemrev.2019.04.001.

Aigaje, E., Riofrio, A., Baykara, H., 2023. Processing, properties, modifications, and environmental impact of nanocellulose/biopolymer composites: a review. Polymers 15, 1219. https://doi.org/10.3390/polym15051219.

Alkhatib, Y., Dewaldt, M., Moritz, S., Nitzsche, R., Kralisch, D., Fischer, D., 2017. Controlled extended octenidine release from a bacterial nanocellulose/poloxamer hybrid system. Eur. J. Pharm. Biopharm. 112, 164–176. https://doi.org/10.1016/j.ejpb.2016.11.025.

Baglo, Y., Sorrin, A.J., Liang, B.J., Huang, H., 2020. Harnessing the potential synergistic interplay between photosensitizer dark toxicity and chemotherapy. Photochem. Photobiol. 96, 636–645. https://doi.org/10.1111/php.13196.

Beekmann, U., Schmölz, L., Lorkowski, S., Werz, O., Thamm, J., Fischer, D., Kralisch, D., 2020. Process control and scale-up of modified bacterial cellulose production for tailor-made anti-inflammatory drug delivery systems. Carbohydr. Polym. 236, 116062. https://doi.org/10.1016/j.carbpol.2020.116062.

Bellmann, T., Luber, R., Kischio, L., Karl, B., Pötzinger, Y., Beekmann, U., Kralisch, D., Wiegand, C., Fischer, D., 2022. Bacterial nanocellulose patches as a carrier for hydrating formulations to improve the topical treatment of nail diseases. Int. J. Pharm. 628, 122267. https://doi.org/10.1016/j.ijpharm.2022.122267.

Bellmann, T., Thamm, J., Beekmann, U., Kralisch, D., Fischer, D., 2023. In situ formation of polymer microparticles in bacterial nanocellulose using alternative and sustainable solvents to incorporate lipophilic drugs. Pharmaceutics 15, 559. https://doi.org/10.3390/pharmaceutics15020559.

Björklund, S., Engblom, J., Thuresson, K., Sparr, E., 2013. Glycerol and urea can be used to increase skin permeability in reduced hydration conditions. Eur. J. Pharm. Sci. 50, 638–645. https://doi.org/10.1016/j.ejps.2013.04.022.

Calzavara-Pinton, P., Rossi, M.T., Sala, R., Venturini, M., 2012. Photodynamic antifungal chemotherapy†. Photochem. Photobiol. 88, 512–522. https://doi.org/10.1111/j.1751-1097.2012.01107.x.

Carrer, V., Alonso, C., Pont, M., Zanuy, M., Córdoba, M., Espinosa, S., Barba, C., Oliver, M.A., Martí, M., Coderch, L., 2020. Effect of propylene glycol on the skin penetration of drugs. Arch. Dermatol. Res. 312, 337–352. https://doi.org/10.1007/s00403-019-02017-5.

Celleno, L., 2018. Topical urea in skincare: a review. Dermatol. Ther. 31, e12690. https://doi.org/10.1111/dth.12690.

Chouhan, P., Saini, T.R., 2012. Hydration of nail plate: a novel screening model for transungual drug permeation enhancers. Int. J. Pharm. 436, 179–182. https://doi.org/10.1016/j.ijpharm.2012.06.020.

D20 Committee, n.d. Test Method for Transparency of Plastic Sheeting. https://doi.org/10.1520/D1746-15.

De Monte Vidal, V., Otero, X.G., Tomé, V.D., Viaño, I.S., Rodríguez, S.C., Igea, S.A., Lajarin-Reinares, M., Herrero, M., Camprodo, X.J., Otero Espinar, F.J., 2026. Optimization of nail therapies: the role of microstructure in the absorption and efficacy of topical treatments. Int. J. Pharm. 697, 126861. https://doi.org/10.1016/j.ijpharm.2026.126861.

Eckl, D.B., Dengler, L., Nemmert, M., Eichner, A., Bäumler, W., Huber, H., 2018. A closer look at dark toxicity of the photosensitizer TMP yP in bacteria. Photochem. Photobiol. 94, 165–172. https://doi.org/10.1111/php.12846.

Elsayed, M.M.A., 2015. Development of topical therapeutics for management of onychomycosis and other nail disorders: a pharmaceutical perspective. J. Control. Release 199, 132–144. https://doi.org/10.1016/j.jconrel.2014.11.017.

Fedeli, S., Paoli, P., Brandi, A., Venturini, L., Giambastiani, G., Tuci, G., Cicchi, S., 2015. Azido-substituted bodipy dyes for the production of fluorescent carbon nanotubes. Chem. – Eur J. 21, 15349–15353. https://doi.org/10.1002/chem.201501817.

Gupta, A.K., Foley, K.A., 2019. Evidence for biofilms in onychomycosis. G. Ital. Dermatol. Venereol. 154. https://doi.org/10.23736/S0392-0488.18.06001-7.

Gupta, A.K., Polla Ravi, S., Choi, S.Y., Konda, A., Cooper, E.A., 2023. Strategies for the enhancement of nail plate permeation of drugs to treat onychomycosis. J. Eur. Acad. Dermatol. Venereol. 37, 243–255. https://doi.org/10.1111/jdv.18638.

Hestrin, S., Schramm, M., 1954. Synthesis of cellulose by *Acetobacter xylinum* . 2. Preparation of freeze-dried cells capable of polymerizing glucose to cellulose. Biochem. J 58, 345–352. https://doi.org/10.1042/bj0580345.

Heydorn, R.L., Lammers, D., Gottschling, M., Dohnt, K., 2023. Effect of food industry by-products on bacterial cellulose production and its structural properties. Cellul. 30, 4159–4179. https://doi.org/10.1007/s10570-023-05097-9.

Higuchi, T., 1963. Mechanism of sustained-action medication. theoretical analysis of rate of release of solid drugs dispersed in solid matrices. J. Pharm. Sci. 52, 1145–1149. https://doi.org/10.1002/jps.2600521210.

Higuchi, T., 1961. Rate of release of medicaments from ointment bases containing drugs in suspension. J. Pharm. Sci. 50, 874–875. https://doi.org/10.1002/jps.2600501018.

Houang, J., Halliday, C., Chen, S., Ho, C., Bekmukhametova, A., Lauto, A., 2021. Effective photodynamic treatment of *Trichophyton* species with Rose Bengal. J. Biophotonics 14, e202000340. https://doi.org/10.1002/jbio.202000340.

Hoy, N.Y., Leung, A.K.C., Metelitsa, A.I., Adams, S., 2012. New concepts in median nail dystrophy, onychomycosis, and hand, foot, and mouth disease nail pathology. ISRN Dermatol. 2012, 1–5. https://doi.org/10.5402/2012/680163.

Huang, X., Brazel, C.S., 2001. On the importance and mechanisms of burst release in matrix-controlled drug delivery systems. J. Control. Release 73, 121–136. https://doi.org/10.1016/S0168-3659(01)00248-6.

ICH, 2023. International council for harmonisation of technical requirements for pharmaceuticals for human use [WWW Document]. ICH Guidel. Q2R2 Valid. Anal. Proced. URL https://www.ema.europa.eu/en/documents/scientific-guideline/ich-q2r2-guideline-validation-analytical-procedures-step-5-revision-2_en.pdf (Accessed 3.24.26).

Jaworek, A.K., Hałubiec, P., Wojas-Pelc, A., Szepietowski, J.C., 2025. Analysis of causative factors and potential predictors of onychomycosis: a retrospective single-center study in Poland. J. Fungi 11, 131. https://doi.org/10.3390/jof11020131.

Jozala, A.F., De Lencastre-Novaes, L.C., Lopes, A.M., De Carvalho Santos-Ebinuma, V., Mazzola, P.G., Pessoa-Jr, A., Grotto, D., Gerenutti, M., Chaud, M.V., 2016. Bacterial nanocellulose production and application: a 10-year overview. Appl. Microbiol. Biotechnol. 100, 2063–2072. https://doi.org/10.1007/s00253-015-7243-4.

Karl, B., Alkhatib, Y., Beekmann, U., Bellmann, T., Blume, G., Steiniger, F., Thamm, J., Werz, O., Kralisch, D., Fischer, D., 2020. Development and characterization of bacterial nanocellulose loaded with Boswellia serrata extract containing nanoemulsions as natural dressing for skin diseases. Int. J. Pharm. 587, 119635. https://doi.org/10.1016/j.ijpharm.2020.119635.

Kinnunen, T., Koskela, M., 1991. Antibacterial and antifungal properties of propylene glycol, hexylene glycol, and 1,3-butylene glycol in vitro. Acta Derm. Venereol. 71, 148–150. https://doi.org/10.2340/0001555571148150.

Klemm, D., Schumann, D., Kramer, F., Heßler, N., Hornung, M., Schmauder, H.-P., Marsch, S., 2006. Nanocelluloses as innovative polymers in research and application. In: Klemm, D. (Ed.), Polysaccharides II, Advances in Polymer Science. Springer Berlin Heidelberg, Berlin, Heidelberg, pp. 49–96. https://doi.org/10.1007/12_097.

Leung, A.K.C., Lam, J.M., Leong, K.F., Hon, K.L., Barankin, B., Leung, A.A.M., Wong, A. H.C., 2020. Onychomycosis: an updated review. Recent Pat. Inflamm. Allergy Drug Discov. 14, 32–45. https://doi.org/10.2174/1872213X13666191026090713.

Li, J., Xue, X., Chen, T., Liang, H., Wang, Y., Xue, M., Ge, J., Wang, P., 2026. Heavy-atom-effect enhanced singlet oxygen generation of carbon dots for lipid-targeting tumor photodynamic therapy inducing ferroptosis. Biomaterials 324, 123525. https://doi.org/10.1016/j.biomaterials.2025.123525.

Liu, D., Labas, A., Long, B., McKnight, S., Xu, C., Tian, J., Xu, Y., 2023. Bacterial nanocellulose production using cost-effective, environmentally friendly, acid whey based approach. Bioresour. Technol. Rep. 24, 101629. https://doi.org/10.1016/j.biteb.2023.101629.

Lusiana, Reichl, S., Müller-Goymann, C.C., 2011. Keratin film made of human hair as a nail plate model for studying drug permeation. Eur. J. Pharm. Biopharm. 78, 432–440. https://doi.org/10.1016/j.ejpb.2011.01.022.

Malallah, O.S., Coleman, L., Nasereddin, S.M., Lockhat, M., Chen, T., Jones, S.A., 2024. Systematic review and QSPR analysis of chemical penetration through the nail to inform onychomycosis candidate selection. Drug Discov. Today 29, 103844. https://doi.org/10.1016/j.drudis.2023.103844.

Maldonado-Carmona, N., Ouk, T.-S., Calvete, M.J.F., Pereira, M.M., Villandier, N., Leroy-Lhez, S., 2020. Conjugating biomaterials with photosensitizes: advances and perspectives for photodynamic antimicrobial chemotherapy. Photochem. Photobiol. Sci. 19, 445–461. https://doi.org/10.1039/c9 pp00398c.

Marques, M.J.D.A.M., Alves, F., Sousa, M., Guimarães, F., Kurachi, C., 2025. Photodynamic and sonophotodynamic inactivation of rhyzopus oryzae biofilm. Photodiagn. Photodyn. Ther. 56, 104972. https://doi.org/10.1016/j.pdpdt.2025.104972.

Moritz, S., Wiegand, C., Wesarg, F., Hessler, N., Müller, F.A., Kralisch, D., Hipler, U.-C., Fischer, D., 2014. Active wound dressings based on bacterial nanocellulose as drug delivery system for octenidine. Int. J. Pharm. 471, 45–55. https://doi.org/10.1016/j.ijpharm.2014.04.062.

Müller, A., Ni, Z., Hessler, N., Wesarg, F., Müller, F.A., Kralisch, D., Fischer, D., 2013. The biopolymer bacterial nanocellulose as drug delivery system: investigation of drug loading and release using the model protein albumin. J. Pharm. Sci. 102, 579–592. https://doi.org/10.1002/jps.23385.

National Library of Medicine, 2025. ClinicalTrials.gov [WWW Document]. ClinicalTrials.gov. URL https://clinicaltrials.gov/ (Accessed 12.11.25).

Navarro-Bielsa, A., Gracia-Cazaña, T., Robres, P., Lopez, C., Calvo-Priego, M.D., Aspiroz, C., Gilaberte, Y., 2022. Combination of photodynamic therapy and oral antifungals for the treatment of onychomycosis. Pharmaceuticals 15, 722. https://doi.org/10.3390/ph15060722.

Nguyen, H.X., Kim, Y., Kekatpure, T.D., Lesica, E., Banga, A.K., 2021. A novel technique to evaluate nail softening effects of different urea formulations. Pharm. Dev. Technol. 26, 403–411. https://doi.org/10.1080/10837450.2021.1881113.

OECD, 2004. Guidance Document for the Conduct of Skin Absorption Studies, OECD Series on Testing and Assessment. OECD. https://doi.org/10.1787/9789264078796-en.

Pötzinger, Y., Rahnfeld, L., Kralisch, D., Fischer, D., 2019. Immobilization of plasmids in bacterial nanocellulose as gene activated matrix. Carbohydr. Polym. 209, 62–73. https://doi.org/10.1016/j.carbpol.2019.01.009.

Queller, J., Bhatia, N., 2015. The Dermatologist's Approach to Onychomycosis. J. Fungi 1, 173–184. https://doi.org/10.3390/jof1020173.

Sahoo, B., Goyal, R., Dutta, S., Joshi, P., Sanyal, K., 2025. *Candida albicans:* insights into the biology and experimental innovations of a commonly isolated human fungal pathogen. ACS Infect. Dis. 11, 1780–1815. https://doi.org/10.1021/acsinfecdis.5c00079.

Schaberle, F.A., 2018. Assessment of the actual light dose in photodynamic therapy. Photodiagn. Photodyn. Ther. 23, 75–77. https://doi.org/10.1016/j.pdpdt.2018.06.009.

Schindelin, J., Arganda-Carreras, I., Frise, E., Kaynig, V., Longair, M., Pietzsch, T., Preibisch, S., Rueden, C., Saalfeld, S., Schmid, B., Tinevez, J.-Y., White, D.J., Hartenstein, V., Eliceiri, K., Tomancak, P., Cardona, A., 2012. Fiji: an open-source platform for biological-image analysis. Nat. Methods 9, 676–682. https://doi.org/10.1038/nmeth.2019.

Shi, Q., Mou, C., Xie, Z., Zheng, M., 2022. Exploring BODIPY derivatives as photosensitizers for antibacterial photodynamic therapy. Photodiagn. Photodyn. Ther. 39, 102901. https://doi.org/10.1016/j.pdpdt.2022.102901.

Siepmann, J., Siepmann, F., 2012. Modeling of diffusion controlled drug delivery. J. Control. Release 161, 351–362. https://doi.org/10.1016/j.jconrel.2011.10.006.

Souza, L.W.F., Souza, S.V.T., Botelho, A.C.D.C., 2014. Distal and lateral toenail onychomycosis caused by Trichophyton rubrum: treatment with photodynamic therapy based on methylene blue dye. An. Bras. Dermatol. 89, 184–186. https://doi.org/10.1590/abd1806-4841.20142197.

Sun, M., Li, D., Xi, Y., Qin, X., Liao, Y., Liu, X., Jia, S., Xie, Y., Zhong, C., 2024. NIR-triggered bacterial cellulose-based wound dressings for multiple synergistic therapy of infected wound. Int. J. Biol. Macromol. 259, 129033. https://doi.org/10.1016/j.ijbiomac.2023.129033.

Täuber, A., Müller-Goymann, C.C., 2015. In vitro permeation and penetration of ciclopirox olamine from poloxamer 407-based formulations – comparison of isolated human stratum corneum, bovine hoof plates and keratin films. Int. J. Pharm. 489, 73–82. https://doi.org/10.1016/j.ijpharm.2015.04.043.

Terbinafine nail solutions for topical treatment of onychomycosis: Ex vivo study on penetration/retention through and into keratin membranes, 2013. J. Am. Acad. Dermatol. 68, AB109. https://doi.org/10.1016/j.jaad.2012.12.452.

Thompson, J.F., Agarwala, S.S., Smithers, B.M., Ross, M.I., Scoggins, C.R., Coventry, B.J., Neuhaus, S.J., Minor, D.R., Singer, J.M., Wachter, E.A., 2015. Phase 2 study of intralesional PV-10 in refractory metastatic melanoma. Ann. Surg. Oncol. 22, 2135–2142. https://doi.org/10.1245/s10434-014-4169-5.

Tricomi, J., Biagiotti, G., Chastel, T., Filiberti, S., Kokot, H., Mancusi, F., Žežlina, M., Rajeh, L., Urbančič, I., Bodin, S., Occhiato, E.G., Turtoi, A., Cicchi, S., Richichi, B., 2025. Synthesis of a water-soluble BODIPY for targeting and assessing the function of endoplasmic reticulum. ACS Bio Med. Chem. Au 5, 895–905. https://doi.org/10.1021/acsbiomedchemau.5c00142.

Vejnovic, I., Simmler, L., Betz, G., 2010. Investigation of different formulations for drug delivery through the nail plate. Int. J. Pharm. 386, 185–194. https://doi.org/10.1016/j.ijpharm.2009.11.019.

Wachter, E., Dees, C., Harkins, J., Scott, T., Petersen, M., Rush, R.E., Cada, A., 2003. Topical rose Bengal: pre-clinical evaluation of pharmacokinetics and safety. Lasers Surg. Med. 32, 101–110. https://doi.org/10.1002/lsm.10138.

Wang, M., Gu, K., Ding, W., Wan, M., Zhao, W., Shi, H., Li, J., 2022. Antifungal effect of a new photosensitizer derived from BODIPY on *Candida albicans* biofilms. Photodiagn. Photodyn. Ther. 39, 102946. https://doi.org/10.1016/j.pdpdt.2022.102946.

Wiegand, C., Moritz, S., Hessler, N., Kralisch, D., Wesarg, F., Müller, F.A., Fischer, D., Hipler, U.-C., 2015. Antimicrobial functionalization of bacterial nanocellulose by loading with polihexanide and povidone-iodine. J. Mater. Sci. - Mater. Med. 26, 245. https://doi.org/10.1007/s10856-015-5571-7.

Wildner, W., Drummer, D., 2019. Nanofiller materials for transparent polymer composites: Influences on the properties and on the transparency—a review. J. Thermoplast. Compos. Mater. 32, 1547–1565. https://doi.org/10.1177/0892705718797157.

Yudianti, R., Syampurwadi, A., Onggo, H., Karina, M., Uyama, H., Azuma, J., 2016. Properties of bacterial cellulose transparent film regenerated from dimethylacetamide-LiCl solution: transparent bacterial cellulose film. Polym. Adv. Technol. 27, 1102–1107. https://doi.org/10.1002/pat.3782.

Zeng, A., Wang, B., Yiasmin, M.N., Yang, R., Tong, Y., Zhao, W., 2024. Next-generation photodynamic antimicrobial materials made by direct synthesis of functional bacterial cellulose. Int. J. Biol. Macromol. 282, 136897. https://doi.org/10.1016/j.ijbiomac.2024.136897.

Zhang, L., Xu, H., Shi, Y., Yu, J., Tao, Y., Li, X., 2018. An exploration of the optimum dosage and number of cycles of itraconazole pulse therapy for severe onychomycosis. Mycoses 61, 736–742. https://doi.org/10.1111/myc.12799.

Zhao, J., Wang, Y., Liu, C., 2022. Film transparency and opacity measurements. Food Anal. Methods 15, 2840–2846. https://doi.org/10.1007/s12161-022-02343-x.